Hindawi
International Journal of Energy Research
Volume 2023, Article ID 5310171, 11 pages
https://doi.org/10.1155/2023/5310171

Research Article

N- and F-Co-Doped Carbon Quantum Dots Coated on a Ni Foam Substrate as Current Collector for Highly Stable Li-Air Batteries

Yuqi Ma, Ki-Wook Sung, and Hyo-Jin Ahn

Department of Materials Science and Engineering, Seoul National University of Science and Technology, Seoul 01811, Republic of Korea

Correspondence should be addressed to Hyo-Jin Ahn; hjahn@seoultech.ac.kr

Received 15 December 2022; Revised 20 January 2023; Accepted 23 January 2023; Published 14 February 2023

Academic Editor: Denis Osinkin

Because of their high theoretical density, Li-air batteries (LABs) are expected to be critical components of future energy storage devices. However, the commercial use of LABs is limited by their low charge-discharge efficiency, high overpotential, and low cyclic stability. Therefore, to improve the cyclic stability of LABs, we manufactured N- and F-co-doped carbon quantum dots (NF-CQDs), thinly coated them on the surface of a Ni foam current collector via ultrasonic spray coating, and used the as-fabricated NF-CQD/Ni as the current collector of an LAB cathode. The NF-CQD/Ni-based cathode maintained remarkable cycling stability over 42 cycles (with a limited capacity was 1000 mAh/g) and exhibited a superior specific discharge capacity of approximately 5121.91 mAh/g (at 100 mA/g). NF-CQD/Ni-based cathode exhibits superior electrochemical properties, including its high cycling stability and high discharge capacity, primarily contributed by the NF-CQD coating layer, which prevented the oxidation of the Ni foam substrate and increased the electrical conductivity and electrocatalytic activity of the cathode. Therefore, NF-CQD/Ni can serve as an excellent current collector for LAB cathodes.

1. Introduction

The greenhouse emitted from burning fossil fuel is one of the primary reasons for global warming becoming increasingly serious. Therefore, considerable efforts have been dedicated to replacing fossil fuels with renewable energy sources [1–3]. Moreover, to meet the need for electric devices, the demand for energy storage devices with excellent safety, stable performance, and high energy density has increased [4, 5]. Li-air batteries (LABs) present an excellent theoretical energy density (11400 Wh/kg) comparable to gasoline (13200 Wh/kg) and are environmentally friendly; therefore, they are expected to be remarkable energy storage systems [6–9]. However, LABs exhibit critical drawbacks, for instance, a high overpotential and low cycling stability, which restrict their practical application [10, 11].

Typical LABs were comprised an electrolyte, a cathode, an anode, and a separator. Discharge-charge process of LABs can be described as follows [12–14]:

$$\begin{aligned}&\text{Discharge process}: \text{oxygen reduction reaction}\\&\cdot\left(\text{ORR}\,;\, 2e^- + 2Li^+ + O_2 \longrightarrow Li_2O_2\right)\\&\text{Charge process}: \text{oxygen evolution reaction}\\&\cdot\left(\text{OER}\,;\, Li_2O_2 \longrightarrow 2e^- + 2Li^+ + O_2\right)\end{aligned} \tag{1}$$

In particular, the low cycling stability of LABs is ascribed to the incomplete decomposition and accumulation of Li_2O_2 at the cathode hindering the transfer of O_2 gas to the cathode. Therefore, to improve the cycling stability of LABs, the overpotential during charging should be decreased by improving the electrical conductivity and electrocatalytic activity of the electrode. Various studies have focused on increasing the electrocatalytic activity of LAB cathodes by using cathode materials with high electrical conductivity, such as carbonaceous active materials [15–17], metallic active materials [18, 19], and electrolytes [20, 21]. However, although the current collector plays a critical role by conferring stability and improving the conductivity and adhesion

of the cathode, studies on current collectors have been scarce [22, 23]. Therefore, surface engineering of current collectors to prevent oxidation and increase conductivity is critical for fabricating highly stable LABs with excellent cycling stability.

In this context, we coated a Ni foam substrate with carbon quantum dots codoped with N and F (NF-CQDs) and used the fabricated sample as the current collector of an LAB cathode. In addition, we estimated the effect of surface engineering on the cycling performances of LABs. Especially, the fabricated NF-CQDs presented large specific surface area, small molecular weight and particle size, high electrical conductivity, and remarkable chemical stability and were synthesized using a simple method. Furthermore, heteroatom doping of CQDs can increase the electrical conductivity and electrocatalytic activity of LAB cathodes. Moreover, the current collector fabricated by depositing a NF-CQD coating layer on the surface of a Ni foam current collector can enhance the cycling stability of LABs by preventing the oxidation of the Ni foam by the water vapor or O_2 in air. In addition, because the ultrasonic spray coating method generates fine droplets via the ultrasonic vibration of the spray nozzle, uniform, dense, and thin coating layers can be deposited on the surfaces of current collectors, unlike the coating layers deposited using other coating methods, such as conventional spray coating or dip coating [24–26].

2. Experimental

NF-CQDs were fabricated using a hydrothermal method. Specifically, 4 wt% of urea (Aldrich), 0.6 wt% of sodium fluoride (Aldrich), and 9 wt% of citric acid (Aldrich) were dissolved in deionized water, then moved to a Teflon-lined hydrothermal synthesis autoclave, and heated at 180°C for 6 h. The prepared solution was centrifuged three times at 10000 rpm during 25 min and then dialyzed using a 6–8 kD molecular weight cut-off membrane for 24 h to obtain uniform small-sized particles. The dialysate was dried in a 50°C oven overnight to obtain NF-CQD particles. Furthermore, to confirm the effect of F doping, N-doped CQDs (N-CQDs) were fabricated using the same procedure in the absence of sodium fluoride. Ni foam was coated with NF-CQDs using an ultrasonic spray coating method and a 1 wt% NF-CQD dispersion in N-methyl-2-pyrrolidinone (NMP). The feeding rate of the dispersion, spraying time, and frequency were set at 1 mL/h, 2 min, and 130 kHz, respectively. Pristine Ni foam, N-CQD-coated Ni foam, and NF-CQD-coated Ni foam (with a radius of 0.65 cm) are hereafter denoted as bare Ni, N-CQD/Ni, and NF-CQD/Ni, respectively.

The element distributions, morphology, and structure of the NF-CQDs were determined by energy-dispersive spectroscopy (EDS; NEO ARM, JEOL) apparatus and a transmission electron microscopy (TEM) instrument. Moreover, the absorbance, crystal structure, chemical bonding structure, and surface functional groups of the N-CQDs and NF-CQDs were evaluated using an X-ray diffraction (XRD) instrument, an ultraviolet-visible (UV-vis) spectrophotometer, a Fourier-transform infrared (FT-IR) spectrometer, and an X-ray photoelectron spectroscopy (XPS; VG Multilab2000m) device, respectively. The thickness of the NF-CQD layer coated on the Ni foam substrate was measured using a scanning transmission electron microscopy (STEM; NEO ARM, JEOL) instrument; the morphologies and structure of the cathode material were analyzed using field emission scanning electron microscope (FESEM, EVO10, Carl Zeiss).

To estimate the electrochemical performance of the LAB cathode, we use coin cells (Hohsen Corporation, CR2032) comprising O_2-electrode as a cathode and porous polypropylene membrane (Welcose, Celgard 2400) as the separator; tetraethylene glycol dimethyl ether (TEGDME) dissolves lithium bis(trifluoromethanesulfonyl)imide (LiTESI) as the electrolyte [27] and Li foil (Honjo Chemical) as the anode. The cathodes were fabricated by polyvinylidene difluoride (20 wt%, PVDF; Arkema) as the binder and Ketjen black (80 wt%, KB; ECP-600JD, Infochems Inc.) as the cathode active material. A mixture of KB and PVDF was dispersed in NMP (Aldrich) and then spray-coated onto bare Ni, N-CQD/Ni, and NF-CQD/Ni, which were used as current collectors, followed by drying in a 50°C oven overnight. The loading of KB was 0.08 ± 0.01 mg. The assembling of cells was carried out in an Ar-atmosphere glove box (99.999%), and the O_2 and H_2O contents were maintained below 10 ppm. The assembled battery was aged for 24 h in an O_2-filled battery jig; discharge-charge tests were conducted using a cycler system (WBCS3000M1) in the voltage range of 2.0–4.5 V (vs. Li/Li^+) at 25°C. Furthermore, cycling stability tests were performed with a specific capacity of 1000 mAh/g at a current density of 100 mA/g. Moreover, we used FESEM of bare Ni-, N-CQD/Ni-, and NF-CQD/Ni-based cathodes after the cycling testing to confirm the stability.

3. Results and Discussion

Figure 1(a) shows the schematic of fabrication of NF-CQDs using hydrothermal, and Figure 1(b) shows the ultrasonic spray coating process to preparation of the NF-CQDs coated on Ni foam. The CQDs were synthesized by hydrothermal method, including citric acid as a carbon source and urea as a nitrogen source, as shown in Figure S1. When heated, citric acid reacted with urea to form citric acid amide; then, further heating leads to deamination, dehydration, and dehydrocondensation of citric acid [28]. Sodium fluoride as a fluorine source and F atoms were incorporated into the honeycomb structure of carbon atoms [29]. Ultrasonic spray coating is an efficient method that can be used to produce fine droplets via ultrasonic vibration and deposit uniform and thin coating layers on various substrates [30]. In this study, an NF-CQD dispersion was finely coated on a Ni foam substrate via ultrasonic spray coating. Because the NF-CQDs contained numerous functional groups, the thin and uniform NF-CQD coating layer enhanced the interfacial adhesion between current collector (Ni foam) and active material (KB) [23, 31]. Therefore, after the generating and decomposition of Li_2O_2 during repeated discharging-charging, KB, which served as the active electrode material, maintained the combined structure of the current collector. Moreover, during cycling, Ni foam was oxidized by the water vapor and O_2 in air and corroded by by-products (LiOH or $Li_2(CO_3)$), especially at high potentials (>4 V vs.

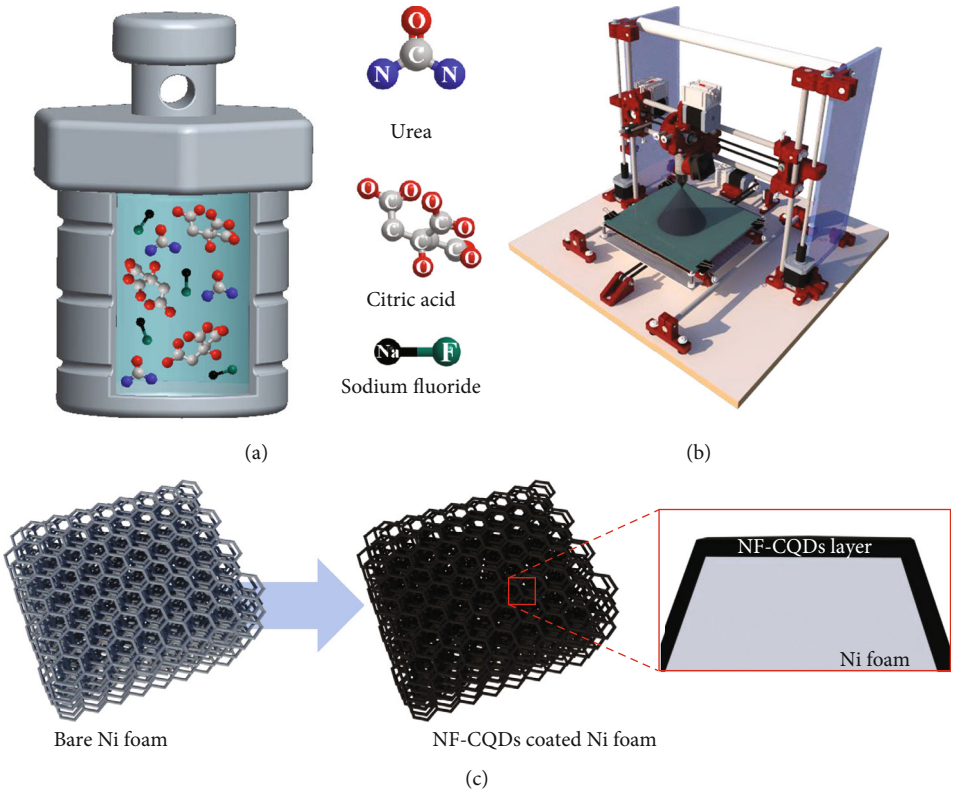

FIGURE 1: Scematics of (a) Fabrication of NF-CQDs using hydrothermal, (b) ultrasonic spray coating preocess, and (c) fabrocated NF-CQDs coated Ni foam by ultrasonic spray coating process.

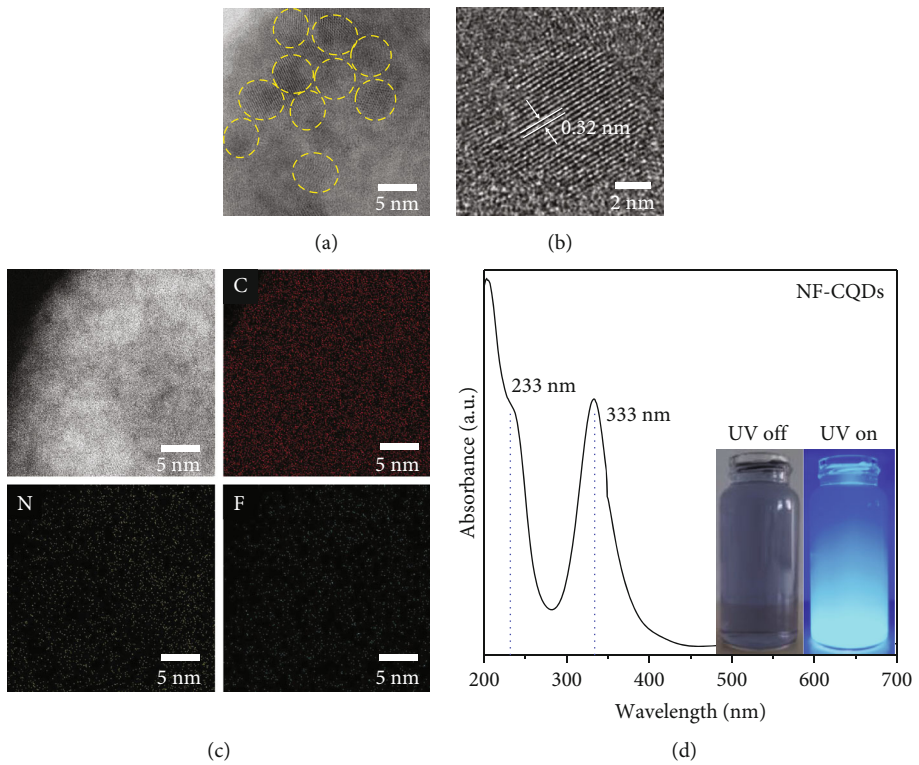

FIGURE 2: (a) Low- and (b) high-resolution TEM images; (c) EDS mapping results of C, N, and F elements of NF-CQDs; (d) UV-vis absorbance spectra with photographs of NF-CQD solution.

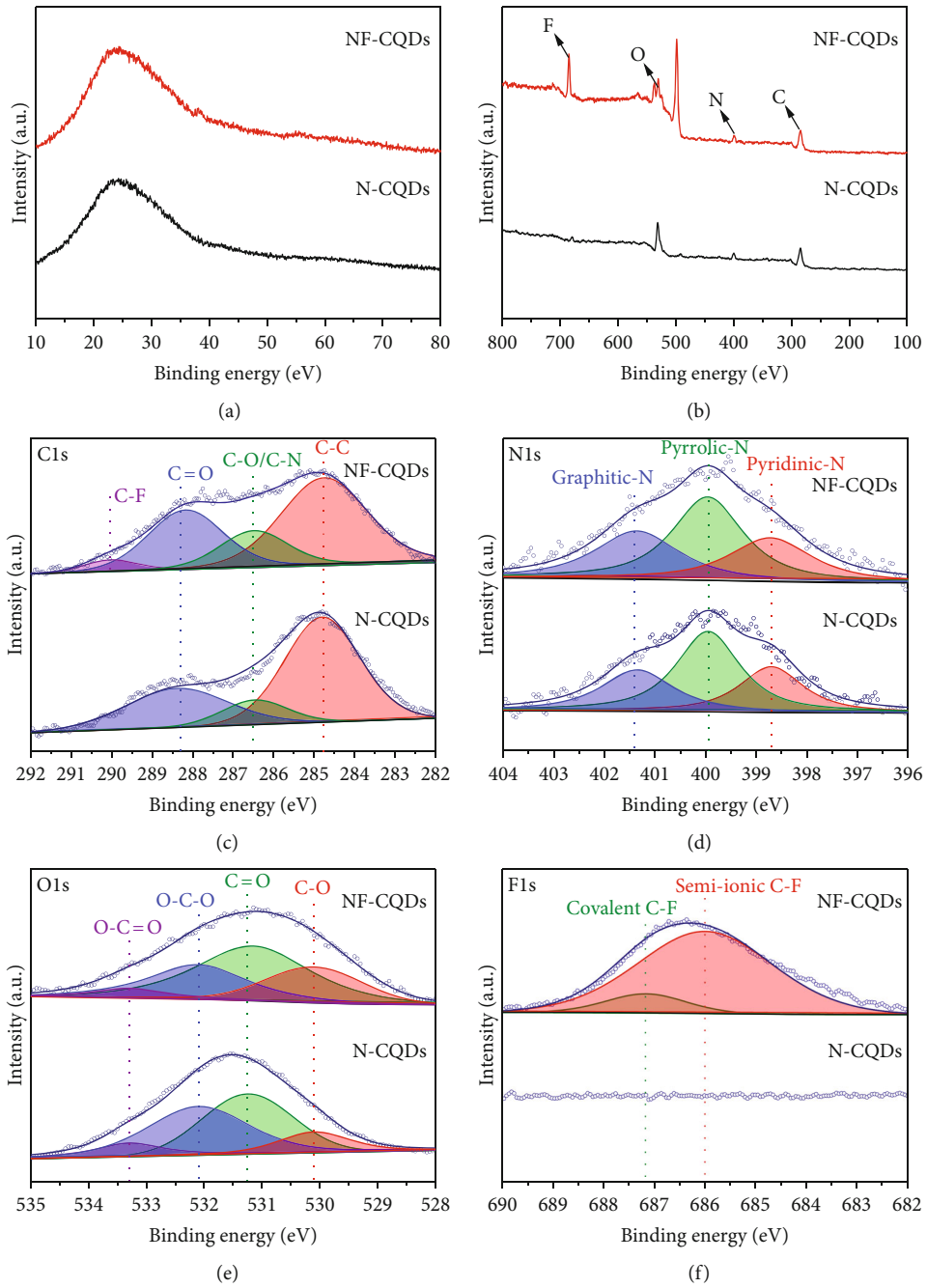

Figure 3: (a) XRD patterns and (b) XPS full spectra, and XPS spectra of (c) C 1s, (d) N 1s, (e) O 1s, and (f) F 1s of N-CQDs and NF-CQDs.

Li/Li^+), which decreased the electrical conductivity of the current collector [32, 33]. However, the NF-CQD coating layer efficiently prevented the oxidation and corrosion of the Ni foam substrate, thereby enhancing the stability of the KB–Ni foam interface [34, 35].

The morphology and element distribution of the NF-CQDs were examined using TEM and EDS mapping. The low- and high-resolution TEM results of NF-CQDs (Figures 2(a) and 2(b)) revealed that the NF-CQDs were ~4.5 nm in diameter and their lattice fringe space was ~0.32 nm, which corresponded to the (002) plane of graphite. To confirm the content distributions of C, O, N, and F, the TEM-EDS mappings of the NF-CQDs were obtained (Figure 2(c)). The EDS data suggested that N and F were present in the NF-CQDs. The UV-vis spectrum and photographs of the NF-CQD dispersion are shown in Figure 2(d) and its inset, respectively. The NF-CQD suspension was grayish blue under natural light (left) and presented royal blue fluoresce under 365 nm UV light irradiation (right). UV-vis absorbance spectra of NF-CQDs included two feature peaks at 333 and 233 nm, which corresponded to $n-\pi^*$ transitions of the C=N and C=C bonds and the $\pi-\pi^*$ transitions of the aromatic sp^2 C atoms of the core domain, respectively [36, 37]. By comparing the UV-vis spectrum of the N-CQDs and

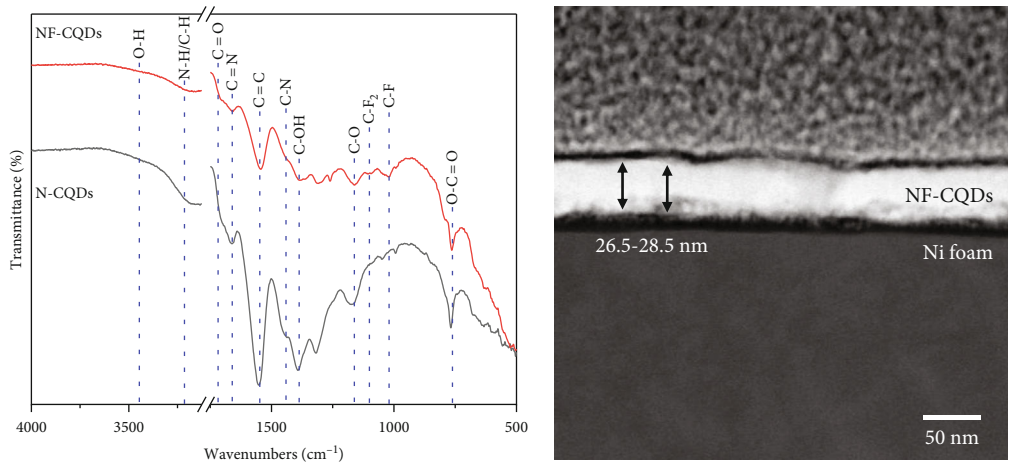

Figure 4: (a) FT-IR spectrum of N-CQDs and NF-CQDs and (b) cross-sectional STEM image of NF-CQD/Ni.

NF-CQDs, it was determined that F doping did not change the characteristic absorption peaks of the CQDs (Figure S2). These results confirmed that we have successfully synthesized NF-CQDs by hydrothermal method.

The XRD was used to examine the structures and phases of N-CQDs and NF-CQDs. The broad peak at 26° in the XRD patterns of N-CQDs and NF-CQDs (Figure 3(a)) was ascribed to the (002) lattice plane of amorphous graphite (JCPDS 65-6212), and these results were consistent with the TEM results [38]. In the XRD results, it was confirmed that the crystal structure of the CQDs was maintained after F doping. Furthermore, the chemical bonding structures of N-CQDs and NF-CQDs were analyzed by XPS, and the results were calibrated with 284.5 eV C 1s binding energy (Figures 3(b)–3(f)). Figure 3(b) displays the XPS survey spectrum of N-CQDs and NF-CQDs having peaks at 282–292, 396–404, 528–535, and 682–690 eV which correspond to the binding energies of C 1s, N 1s, O 1s, and F 1s, indicating that N and F atoms have been successfully doped to CQDs. The C 1s XPS profile of the NF-CQDs included the characteristic peaks of C–F groups (~291.6 eV), O=C groups (~288.6 eV), C–N/C–O groups (~286.7 eV), and C–C groups (~284.8 eV) (Figure 3(c)). In contrast, the characteristic peak of C–F was absent from the C 1s XPS profile of the N-CQDs, indicating that the F atoms were only present in the NF-CQDs. The N 1s XPS profiles of N-CQDs and NF-CQDs (Figure 3(d)) included the characteristic peaks of pyridinic-N (~398.7 eV), pyrrolic-N (~399.9 eV), and graphitic-N (~401.4 eV). The presence of these groups was ascribed to the use of urea, a precursor of the N-CQDs, as the N source. The pyridinic- and pyrrolic-N presented two p-electrons, which originated from their aromatic π-systems and increased the electrical conductivity of the N-CQDs [39, 40]. The O 1s XPS profiles of N-CQDs and NF-CQDs (Figure 3(e)) included the characteristic peaks of C–O (~530.1 eV), C=O (~531.2 eV), O–C–O (~532.1 eV), and O–C=O (~533.3 eV). Furthermore, the F 1s XPS profiles presented two peaks at ~687.2 and~685.9 eV, which corresponded to the covalent and semi-ionic bonds of C–F (Figure 3(f)). These groups were not observed in the F 1s XPS profile of the N-CQDs, indicating that F atoms were only present in the NF-CQDs. The electronegativity of F (4.0) is higher than that of C (2.5); accordingly, the electron/ion conductivity of the NF-CQDs increases because the polar C–F bonds presented a dipole moment [23]. Therefore, owing to F doping, the C atoms of the NF-CQDs became positively charged, and the activity of the π-electrons of the NF-CQDs was higher than that of the π-electrons of the N-CQDs, causing the higher electrocatalytic activity of NF-CQDs than N-CQDs [39]. Consequently, the NF-CQD coating layer increased the electrical conductivity and electrocatalytic activity of the LAB cathode, thereby promoting the decomposition and formation of Li_2O_2 during charging and discharging [41].

Chemical properties of functional groups on the surface of N-CQDs and NF-CQDs were determined by FT-IR spectrum (Figure 4(a)). The characteristic peaks at 776, 1180, 1398, 1448, 1555, 1660, 1718, 3213, and 3445 cm^{-1} in the FT-IR spectrum of N-CQDs and NF-CQDs were attributed to the telescopic vibrations of O=C–O, C–O, C–OH, C–N, C=C, C=N, C=O, N–H/C–H, and O–H bonds and functional groups, respectively. The characteristic peaks at 1020 and 1104 cm^{-1} in the FT-IR spectrum of NF-CQDs were attributed to the telescopic vibrations of C–F and C–F_2, respectively [42–44]. The characteristic peak of the C–N bonds in the FT-IR spectroscopy of the NF-CQDs confirmed that the CQDs were doped with N atoms. Moreover, the presence of the characteristic peaks of the C=N and C=C bonds indicated that the hydrothermally synthesized NF-CQDs presented a hetero-polyaromatic structure. The characteristic peaks of C–F_2 and C–F in the FT-IR spectrum of the NF-CQDs suggested that the CQDs were doped with F atoms. These results were consistent with the aforementioned XPS spectra. Furthermore, STEM results demonstrated that the NF-CQD coating layer was uniform and thin (26.5–28.5 nm) (Figure 4(b)). Because the NF-CQDs surface exist a great quantity of oxygen containing functional groups, the NF-CQD coating layer strongly interacted with the Ni foam

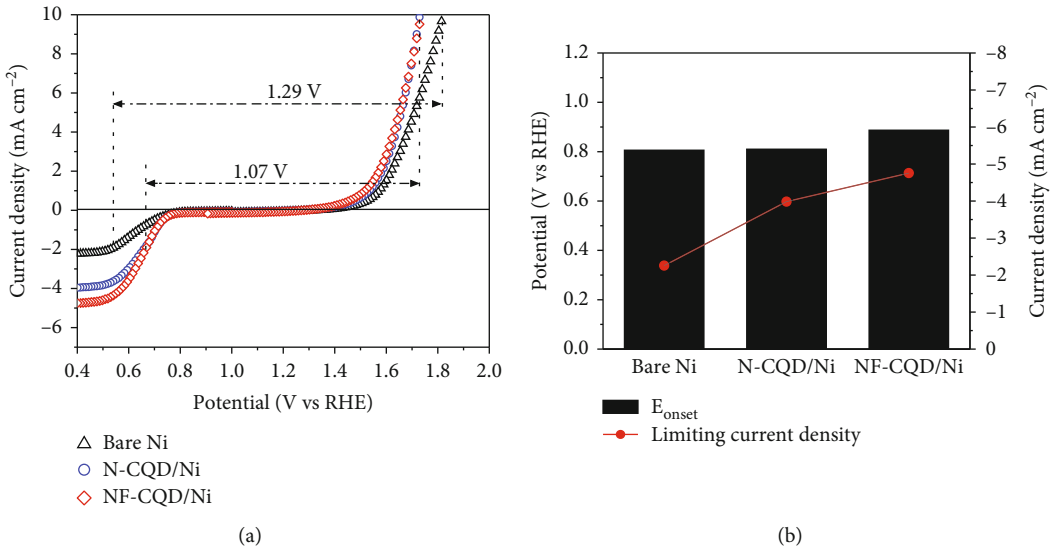

Figure 5: (a, b) LSV curves of ORR and OER electrocatalytic activity for bare Ni, N-CQD/Ni, and NF-CQD/Ni-based cathode.

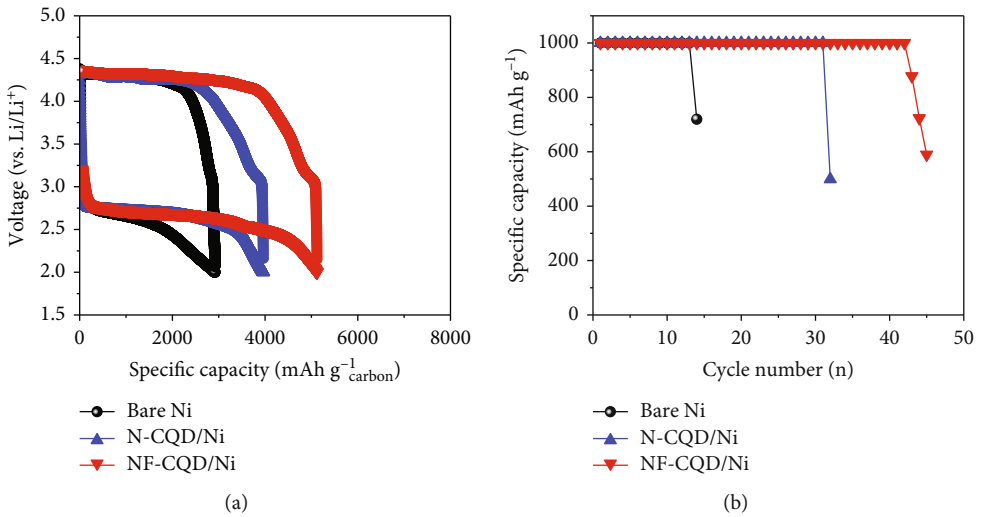

Figure 6: (a) Initial galvanostatic discharging/charging curves at the current density of 100 mA/g and (b) cycling stability at a limited capacity of 1000 mAh/g and a current density of 100 mA/g of bare Ni, N-CQD/Ni, and NF-CQD/Ni-based cathode.

substrate, enhancing the adhesion between KB and Ni foam. Furthermore, the morphology of the Ni foam substrate did not change after N-CQD and NF-CQD coating via ultrasonic spraying (Figure S3). Moreover, the uniform and thin CQD coating layers effectively prevented the oxidation of Ni foam during cycling. Therefore, these findings confirmed that the NF-CQD coating layer enhanced the cycling stability of LABs.

To assess the electrochemical catalytic activities of the bare Ni, N-CQD/Ni, and NF-CQD/Ni electrodes, LSV measurements were carried out (Figure 5). LAB cathodes involve two key reactions: ORR and OER. They all involve multistep electron transfer processes with inherently slow kinetics [45]. In the ORR polarization curve region, the onset potential of NF-CQD/Ni (0.887 V) was higher than that of other electrodes (N-CQD/Ni: 0.81 V and bare Ni: 0.806 V), implying that the NF-CQD/Ni has high ORR catalytic activity. The limiting current density of NF-CQD/Ni-based cathode (-4.755 mA cm^{-2}) was superior then that of bare Ni and N-CQD/Ni-based electrodes (-2.256 and -3.985 mA cm^{-2}, respectively) as shown in Figure 5(b). This result was ascribed to that F atoms can improve the ionic/conductivity of the interfacial layer. In the OER polarization curve region, the NF-CQD/Ni- and N-CQD/Ni-based electrodes showed the superior negative E_{onset}, exhibiting excellent OER catalytic performance. During the discharge-charge process of LABs, the ORR and OER electrochemical kinetics are crucial; they are generally evaluated by the potential gap ($E_{OER-ORR}$) between OER (at 10 mA cm^{-2}) and ORR (at -2 mA cm^{-2}) [46]. The NF-CQD/Ni-based and N-CQD/Ni-based electrodes showed a potential difference of 1.07 V,

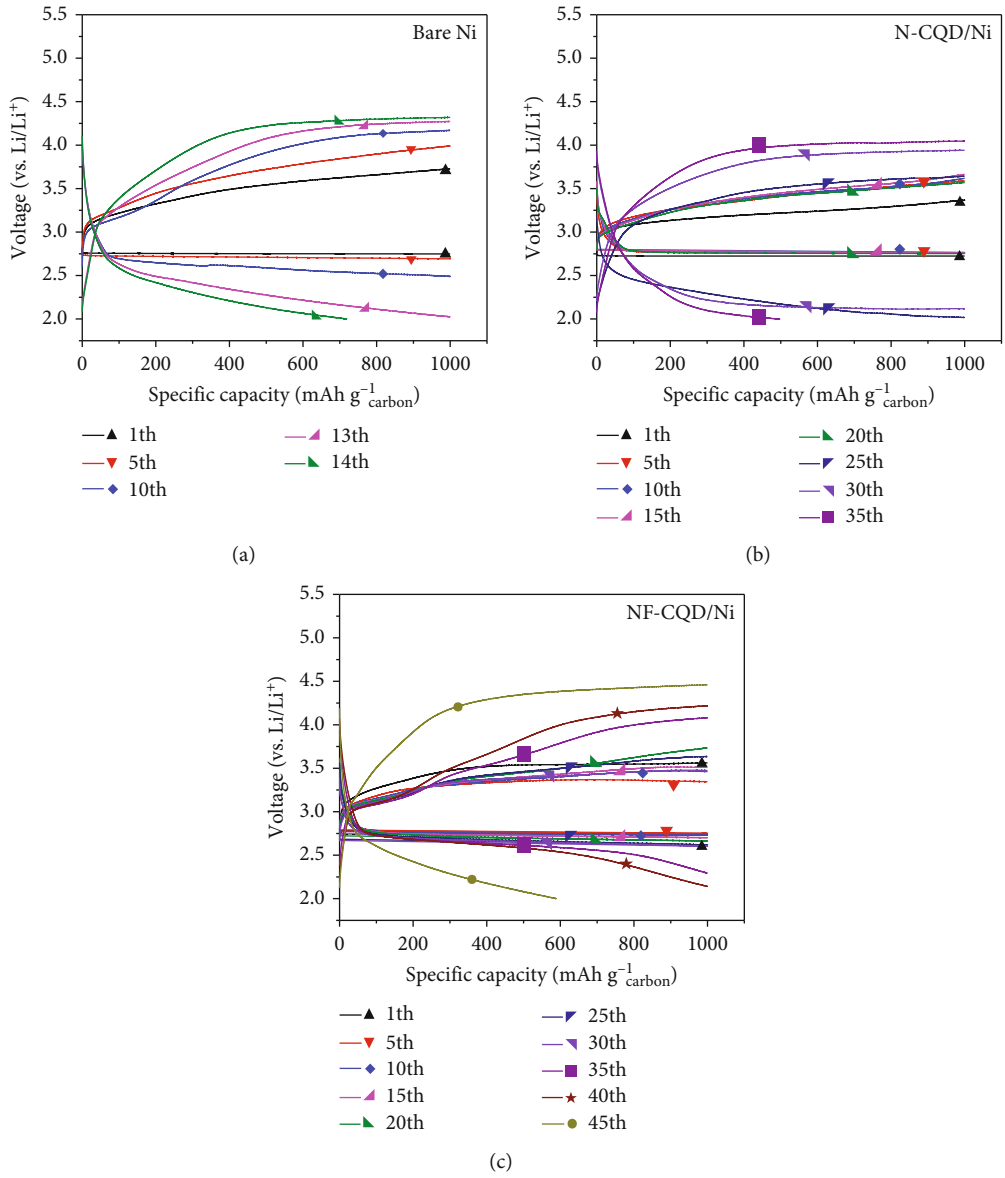

Figure 7: Specific capacity-limited discharging/charging profiles of first and every five cycles at a limited capacity of 1000 mAh/g and a current density of 100 mA/g of (a) bare Ni, (b) N-CQD/Ni, and (c) NF-CQD/Ni-based cathode.

which may be due to the efficient electron transport due to the oxygen reaction promoted by N doping.

To assess the cathode electrochemical performance, we fabricated cathodes by coating KB as the active material on bare Ni, N-CQD/Ni, and NF-CQD/Ni current collectors. The initial constant current discharge-charge curves of the fabricated cathodes are displayed on Figure 6 over a current density of 100 mA/g in the voltage range of 2.0–4.5 V. The initial specific capacities of the bare Ni-based cathode (2917.97 mAh/g) were lower than that of the N-CQD/Ni- and NF-CQD/Ni-based cathodes (3963.52 and 5121.91 mAh/g, respectively). Furthermore, the discharge-charge voltage gap of the NF-CQD/Ni-based cathode (1.603 V at 2000 mAh/g) was narrower than that of the bare Ni-based cathode (1.771 V at 2000 mAh/g). This result was ascribed to the higher ORR and OER electrocatalytic activities of the NF-CQD/Ni-based cathode than the bare Ni-based cathode during charging, which promoted the efficient decomposition of Li_2O_2. The cycling stability of the fabricated cathodes was assessed at a limited capacity of 1000 mAh/g, at a current density of 100 mA/g, and in the voltage range of 2.0–4.5 V (Figure 6(b)). The cycling stability of the NF-CQD/Ni-based cathode (42 cycles) was superior to those of the bare Ni- and N-CQD/Ni-based cathodes (13 and 31 cycles, respectively). During the discharging-charging test, Li_2O_2 formed continuously as the product of the discharging reaction and decomposed at the cathode surface, thereby lowering the cycling stability of the LAB. In particular, the cycling stability of the LABs featuring the NF-CQD-based cathode was higher than those of the other LABs because F doping caused the electrochemical catalytic activity and electrical conductivity of the electrode to increase, thereby inducing the efficient decomposition of Li_2O_2. For the N-CQD/Ni- and NF-CQD/Ni-based

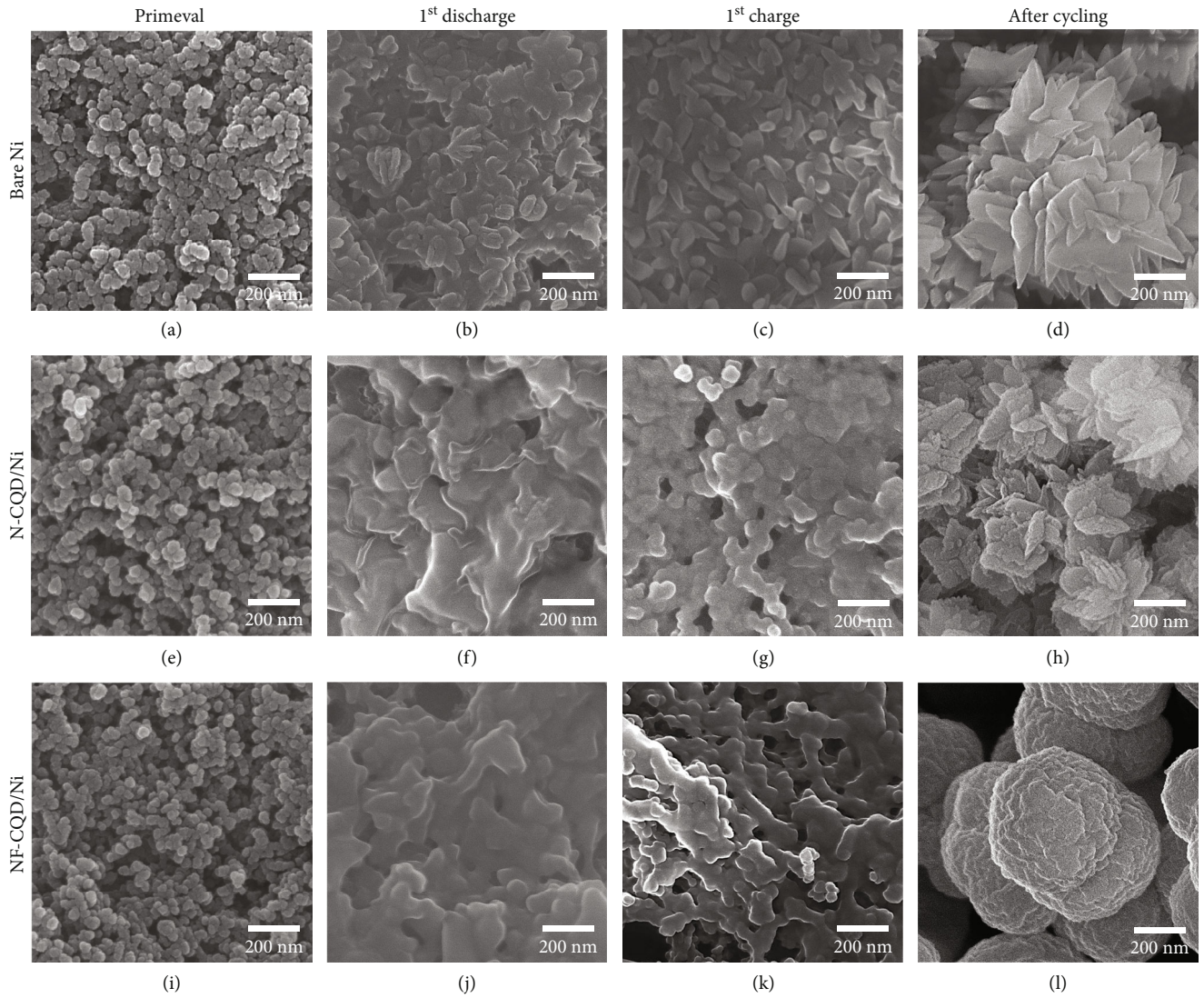

Figure 8: FESEM images of cathode fabricated with (a–d) bare Ni, (e–h) N-CQD/Ni, and (i–l) NF-CQD/Ni primeval, after 1st discharging, 1st recharging, and cycling test.

cathodes, the CQD coating layers suppressed the oxidation of the Ni foam substrates, which improved the cycling stabilities of the corresponding LABs. Moreover, compared with other reported electrodes without carbon coating, the NF-CQD/Ni-based cathode exhibits excellent performance in terms of specific capacity and cycle stability (Table S1) [47–50].

The discharge-charge voltage curve of bare Ni-, N-CQD/Ni-, and NF-CQD/Ni-based cathodes are shown in Figure 7. The bare Ni-based cathode exhibited a stable discharging-charging voltage gap during the first five cycles (Figure 7(a)). However, after 10 cycles, the charging overpotential of the bare Ni-based cathode increased slowly, causing a decrease in discharge capacity. In contrast, the N-CQD/Ni-based cathode presented a stable voltage gap for 25 cycles. This was attributed by the increase in the conductivity of the N-CQD coating layer induced by N doping, which promoted the ORR and OER at the cathode. Furthermore, the NF-CQD/Ni-based cathode presented excellent cycling stability and a stable voltage gap for 30 cycles. These results were ascribed to the F doping of the NF-CQD coating layer; the electrocatalytic activity of the cathode materials is increased by increasing the activity of the π-electrons of N-CQDs. Therefore, for the bare Ni-based cathode with a low electrocatalytic activity, Li_2O_2 was only partially decomposed, and it accumulated at the surface of the cathode, causing a decrease in its electrical conductivity. Thereby, the ORR and OER at the bare Ni-based cathode were disturbed, and the cycling stability of the cathode was poor. However, the NF-CQD coating layer prevented the oxidation of the Ni foam substrate and promoted the efficient decomposition of Li_2O_2 by increasing catalytic activity and conductivity efficiency of electrodes, thereby increasing the cycling capability of the cathode [51, 52].

To compare the cycling stabilities of the electrodes after the discharge-charge tests, we analyzed the FESEM of the bare Ni-, N-CQD/Ni-, and NF-CQD/Ni-based cathodes before first discharging, after first discharging and charging, and after the cycling stability tests (Figure 8). Before first discharging, bare Ni-, N-CQD/Ni-, and NF-CQD/Ni-based

Table 1: EDS element images for the cathode of bare Ni, N-CQD/Ni, and NF-CQD/Ni primeval, after 1st discharging, 1st recharging, and cycling test.

Status	Cathode	Chemical composition (at%) C	O
Primeval	Bare Ni	100	0
	N-CQD/Ni	100	0
	NF-CQD/Ni	100	0
1st discharge	Bare Ni	25.65	74.35
	N-CQD/Ni	45.05	54.95
	NF-CQD/Ni	50.65	49.35
1st charge	Bare Ni	34.78	65.22
	N-CQD/Ni	58.47	41.53
	NF-CQD/Ni	76.26	23.74
After cycling	Bare Ni	17.09	82.91
	N-CQD/Ni	19.13	80.87
	NF-CQD/Ni	29.97	70.03

cathodes showed uniform KB particles (Figures 8(a), 8(e), and 8(i)). The products which were formed at first discharging process on the bare Ni cathode were peony flower-like (Figure 8(b)), but they were not completely decomposed after charging (Figure 8(c)). Compared with bare/Ni, the particles on the surface of N-CQD/Ni- and NF-CQD/Ni-based cathodes did not exhibit peony flower-like morphology after first discharging, and they showed the decomposed discharge products and decreased particle size after first charging (Figures 8(f), 8(g), 8(j), and 8(k)). Also, the particles on the surface of N-CQD/Ni- and NF-CQD/Ni-based electrodes were sticky compared to bare Ni electrodes after charge-discharge tests because the N-CQDs and NF-CQDs coated on Ni foam enhance cycling stability by the strong connection between the current collector and electrode. The discharge product of LABs is Li_2O_2; however, the X-ray energy of Li (52 eV) is too small to be distinguished by EDS, so we analyzed the percentages of the O element to confirm the discharge product content on the surface of electrodes (Table 1). After the first discharge, the atomic percent of O element in the NF-CQD/Ni (49.35 at%) was smaller than others (74.35 at% of bare Ni and 54.95 at% of N-CQD/Ni), but after charging, the atomic percentage of NF-CQD/Ni was only 23.74 at% (65.22 at% of bare Ni and 41.53 at% of N-CQD/Ni). According to the top-view FESEM image of the bare Ni-based cathode, the discharge-charge product comprised peony flower-like Li_2O_2 particles with a 2-D sharp sheet morphology (Figure 8(d)). It has been reported that Li_2O_2 grew heterogeneously on the surfaces of cathodes with low ORR and OER activities. Moreover, the incomplete decomposition of Li_2O_2 caused the accumulation of dense and sharp 2-D Li_2O_2 sheets on the surfaces of cathodes during discharging-charging, thereby interrupting the gas transfer at the cathodes. In contrast, Li_2O_2 grew homogeneously on the surfaces of cathodes with high ORR and OER activities, and the small and spherical Li_2O_2 particles that accumulated at the cathode surfaces were less disruptive for the gas transfer at the cathodes [53, 54]. Therefore, owing to the poor ORR and OER activities of the bare Ni-based cathode, the peony flower-like Li_2O_2 particles grown on its surface caused its cycling stability to decrease by blocking its pores and decreasing its active sites. The Li_2O_2 particles that accumulated at the N-CQD/Ni-based cathode surfaces also presented a peony flower-like structure; however, the 2-D Li_2O_2 sheets were shorter and smaller than those grown on the surface of the bare Ni-based cathode (Figure 8(h)). Moreover, the Li_2O_2 particles deposited on the NF-CQD/Ni-based cathode were spherical with bump surface (Figure 8(l)). The contents of discharge products on surface of electrodes were determined by analyzing the atomic percentage of O element. As shown in Table 1, the atomic percentage of O in bare Ni-based cathode (82.91 at%) was higher than other cathodes after the cycle test (N-CQD/Ni: 80.87 at% and NF-CQD/Ni: 70.03 at%). These results indicated that codoping with N and F caused the ORR and OER activities of NF-CQD/Ni-based cathode to increase, leading to the uniform growth and efficient decomposition of Li_2O_2. Moreover, the hindering effect of the spherical Li_2O_2 particles on the gas transfer at the cathode was lower than that of the 2-D Li_2O_2 sheets; therefore, the NF-CQD coating layer enhanced the cycling stability of the NF-CQD-based cathode.

Therefore, the NF-CQD/Ni-based cathode exhibits highly stable electrochemical performance, which is ascribed to the NF-CQD layer coated on the Ni foam substrate. The NF-CQD/Ni-based cathode exhibits remarkable cycling stability due to the following: (a) the NF-CQD coating layer prevented the oxidation of the Ni foam substrate during discharging–charging, and (b) the NF-CQDs increased the electrical conductivity and electrocatalytic activity of the cathode, facilitating the efficient decomposition of Li_2O_2.

4. Conclusion

In this study, we fabricated a NF-CQD/Ni-based cathode for highly stable LABs using a hydrothermal method followed by ultrasonic spray coating. The NF-CQD/Ni-based cathode displayed an excellent initial discharge capacity of 5121.91 mAh/g at a current density of 100 mA/g, a low discharge-charge voltage gap of 1.603 V at 2000 mAh/g, and outstanding cycling stability over 42 cycles (with a limited capacity of 1000 mAh/g). These results are attributed to the effect of the NF-CQD coating on the Ni foam substrate as follows: (i) the NF-CQD coating layer prevented the oxidation of the Ni foam matrix and (ii) co-doping with N and F improved the electrocatalytic activity and electrical conductivity of the cathode. We believe that coating NF-CQD layers on current collectors can be used to fabricate highly stable LABs.

Data Availability

The data used to support the findings of this study are included within the manuscript and the supplementary information files.

Conflicts of Interest

The authors declare that they have no conflicts of interest.

Authors' Contributions

Yuqi Ma and Ki-Wook Sung contributed equally to this work.

Acknowledgments

This work was supported by the National Research Foundation of Korea (NRF) grant funded by the Korea government (MSIT) (No. 2019R1 A2 C1005836).

Supplementary Materials

Figure S1: the kinetic mechanism of the formation of CQDs. Figure S2: UV-vis absorbance spectrum of N-CQDs. Figure S3: FESEM images of (a, d) bare Ni, (b, e) N-CQD/Ni, and (c, f) NF-CQD/Ni. Table S1: specific capacity and cycle stability of without carbon coating electrodes reported previously. *(Supplementary Materials)*

References

[1] J. Lu, L. Li, J.-B. Park, Y. K. Sun, F. Wu, and K. Amine, "Aprotic and aqueous Li-O_2 batteries," *Chemical Reviews*, vol. 114, no. 11, pp. 5611–5640, 2014.

[2] S. Bilgen, "Structure and environmental impact of global energy consumption," *Renewable and Sustainable Energy Reviews*, vol. 38, pp. 890–902, 2014.

[3] D. Ibrahim, "Renewable energy and sustainable development: a crucial review," *Renewable and Sustainable Energy Reviews*, vol. 4, pp. 157–175, 2000.

[4] G. Girishkumar, B. McCloskey, A. Luntz, S. Swanson, and W. Wilcke, "Lithium-air battery: promise and challenges," *Journal of Physical Chemistry Letters*, vol. 1, no. 14, pp. 2193–2203, 2010.

[5] Y. Zhang, L. Wang, Z. Guo, Y. Xu, Y. Wang, and H. Peng, "High-performance lithium–air battery with a coaxial-fiber architecture," *Angewandte Chemie, International Edition*, vol. 55, no. 14, pp. 4487–4491, 2016.

[6] Y. Yao, J. Cao, W. Yin, Q. Zhang, L. Yang, and X. Wei, "Modified graphene sheets as promising cathode catalysts for Li-O_2 batteries: a first-principles study," *Journal of Physical Chemistry C*, vol. 125, no. 8, pp. 4363–4370, 2021.

[7] K. Surya, M. Michael, and S. Prabaharan, "A review on advancement in non-noble metal based oxides as bifunctional catalysts for rechargeable non-aqueous Li/air battery," *Solid State Ionics*, vol. 317, pp. 89–96, 2018.

[8] P. Bruce, S. Freunberger, L. Hardwick, and J. M. Tarascon, "Li-O_2 and Li-S batteries with high energy storage," *Nature Materials*, vol. 11, no. 1, pp. 19–29, 2012.

[9] Y. Shao, F. Ding, J. Xiao et al., "Making Li-air batteries rechargeable: material challenges," *Advanced Functional Materials*, vol. 23, no. 8, pp. 987–1004, 2013.

[10] S. Freunberger, Y. Chen, Z. Peng et al., "Reactions in the rechargeable lithium–O_2 battery with alkyl carbonate electrolytes," *Journal of the American Chemical Society*, vol. 133, no. 20, pp. 8040–8047, 2011.

[11] M. Thotiyl and S. Freunberger, "A stable cathode for the aprotic Li-O_2 battery," *Nature Materials*, vol. 12, no. 11, pp. 1050–1056, 2013.

[12] H.-G. Jo, K.-H. Kim, and H.-J. Ahn, "Nitrogen-doped carbon quantum dots decorated on platinum catalysts for improved oxygen reduction reaction," *Applied Surface Science*, vol. 554, article 149595, p. 149594, 2021.

[13] I. Gunasekara, S. Mukerjee, E. Plichta, M. A. Hendrickson, and K. M. Abraham, "Microelectrode diagnostics of lithium-air batteries," *Journal of the Electrochemical Society*, vol. 161, no. 3, pp. A381–A392, 2014.

[14] X. Ren, S. Zhang, D. Tran, and J. Read, "Oxygen reduction reaction catalyst on lithium/air battery discharge performance," *Journal of Materials Chemistry*, vol. 21, no. 27, pp. 10118–10125, 2011.

[15] M. Carboni, S. Brutti, and A. Marrani, "Surface reactivity of a carbonaceous cathode in a lithium triflate/ether electrolyte-based Li–O_2 cell," *ACS Applied Materials & Interfaces*, vol. 7, no. 39, pp. 21751–21762, 2015.

[16] S. V. Pavlov and S. A. Kislenko, "Effects of carbon surface topography on the electrode/electrolyte interface structure and relevance to Li–air batteries," *Physical Chemistry Chemical Physics*, vol. 18, no. 44, pp. 30830–30836, 2016.

[17] X. Zhu, Y. Wu, W. Wan et al., "CNF-grafted carbon fibers as a binder-free cathode for lithium-oxygen batteries with a superior performance," *International Journal of Hydrogen Energy*, vol. 43, no. 2, pp. 739–747, 2018.

[18] A. N. Marianov and Y. Jiang, "Effect of manganese porphyrin covalent immobilization on electrocatalytic water oxidation and oxygen reduction reactions," *ACS Sustainable Chemistry & Engineering*, vol. 7, no. 4, pp. 3838–3848, 2019.

[19] T. Oh, D. Park, and J. Kim, "$CoFe_2O_4$ nanoparticles anchored on N/S co-doped mesoporous carbon spheres as efficient bifunctional electrocatalysts for oxygen catalytic reactions," *International Journal of Hydrogen Energy*, vol. 44, no. 5, pp. 2645–2655, 2019.

[20] Z. Guo, X. Dong, S. Yuan, Y. Wang, and Y. Xia, "Humidity effect on electrochemical performance of Li-O_2 batteries," *Journal of Power Sources*, vol. 264, pp. 1–7, 2014.

[21] S. Meini, M. Piana, N. Tsiouvaras, A. Garsuch, and H. A. Gasteiger, "The effect of water on the discharge capacity of a non-catalyzed carbon cathode for Li-O_2 batteries," *Electrochemical and Solid-State Letters*, vol. 15, no. 4, pp. A45–A48, 2012.

[22] Z. Luo, C. Liang, F. Wang et al., "Optimizing main materials for a lithium-air battery of high cycle life," *Advanced Functional Materials*, vol. 24, no. 14, pp. 2101–2105, 2014.

[23] D.-Y. Shin, K.-W. Sung, and H.-J. Ahn, "Fluorine-doped carbon quantum dot interfacial layer on stockade-like etched copper foil for boosting Li-ion storage," *Chemical Engineering Journal*, vol. 413, article 127563, 2021.

[24] G.-H. An and H.-J. Ahn, "Excellent electrochemical stability of graphite nanosheet-based interlayer for electric double layer capacitors," *Applied Surface Science*, vol. 473, pp. 77–82, 2019.

[25] A. Dalmoro, A. Barba, G. Lamberti, and M. d'AmoreIntensifying the microencapsulation process: ultrasonic atomization as an innovative approach," *European Journal of Pharmaceutics and Biopharmaceutics*, vol. 80, no. 3, pp. 471–477, 2012.

[26] S. R. Ardekani and A. S. R. Aghdam, "A comprehensive review on ultrasonic spray pyrolysis technique: mechanism, main parameters and applications in condensed matter,"

Journal of Analytical and Applied Pyrolysis, vol. 141, article 104631, 2019.

[27] J. W. Chen, C. G. Chen, and A. S. Yu, "LiTFSI concentration optimization in TEGDME solvent for lithium–oxygen batteries," *ACS Omega*, vol. 4, no. 24, pp. 20708–20714, 2019.

[28] T. Ogi, K. Aishima, and K. Okuyama, "Kinetics of nitrogen-doped carbon dot formation via hydrothermal synthesis," *New Journal of Chemistry*, vol. 40, no. 6, pp. 5555–5561, 2016.

[29] Z. M. Markovic, M. Labudova, and B. M. T. Markovic, "Highly efficient antioxidant F- and cl-doped carbon quantum dots for bioimaging," *ACS Sustainable Chemistry & Engineering*, vol. 8, no. 43, pp. 16327–16338, 2020.

[30] K. O. Vieira, J. Bettini, L. F. de Oliveira, J. L. Ferrari, and M. A. Schiavon, "Synthesis of multicolor photoluminescent carbon quantum dots functionalized with hydrocarbons of different chain lengths," *Carbon*, vol. 32, no. 4, pp. 327–337, 2017.

[31] S. Ammara, S. Shamaila, R. Sharif, S. Ghani, and N. Zafar, "Uniform and homogeneous growth of copper nanoparticles on electrophoretically deposited carbon nanotubes electrode for nonenzymatic glucose sensor," *Acta Metallurgica Sinica*, vol. 29, pp. 889–894, 2016.

[32] J.-G. Zhang, D. Wang, W. Xu, J. Xiao, and R. E. Williford, "Ambient operation of Li/air batteries," *Journal of Power Sources*, vol. 195, no. 13, pp. 4332–4337, 2010.

[33] "Corrosion resistance of nickel foam modified with electroless Ni–P alloy as positive current collector in a lithium ion battery," *RSC Advances*, vol. 3, no. 48, pp. 25648–25651, 2013.

[34] P. Saheeda, K. Sabira, J. Joseph, and S. Jayaleksmi, "Green chemistry route to realize, high quantum yield carbon quantum dots for cellular imaging applications," *Materials Research Express*, vol. 6, no. 7, article 075025, 2019.

[35] V. L. John, Y. Nair, and T. P. Vinod, "Doping and surface modification of carbon quantum dots for enhanced functionalities and related applications," *Particle and Particle Systems Characterization*, vol. 38, no. 11, article 2100170, 2021.

[36] Y. W. Lee, G. H. An, B. S. Kim et al., "Synergistic effects of a multifunctional graphene based interlayer on electrochemical behavior and structural stability," *ACS Applied Materials & Interfaces*, vol. 8, no. 27, pp. 17651–17658, 2016.

[37] S. Bose, S. Keller, T. Alstrøm, A. Boisen, and K. AlmdalProcess optimization of ultrasonic spray coating of polymer films," *Langmuir*, vol. 29, no. 23, pp. 6911–6919, 2013.

[38] C. Zhao, Y. Jiao, F. Hu, and Y. Yang, "Green synthesis of carbon dots from pork and application as nanosensors for uric acid detection," *Spectrochimica Acta. Part A, Molecular and Biomolecular Spectroscopy*, vol. 190, pp. 360–367, 2018.

[39] G. Panomsuwan, N. Saito, and T. Ishizaki, "Simple one-step synthesis of fluorine-doped carbon nanoparticles as potential alternative metal-free electrocatalysts for oxygen reduction reaction," *Journal of Materials Chemistry A*, vol. 3, no. 18, pp. 9972–9981, 2015.

[40] H.-G. Jo, K.-H. Kim, and H.-J. Ahn, "Well-dispersed Pt/RuO_2-decorated mesoporous N-doped carbon as a hybrid electrocatalyst for Li–O_2 batteries," *RSC Advances*, vol. 11, no. 20, pp. 12209–12217, 2021.

[41] C. Liang, H. Y. Niu, and H. P. Feng, "Efficient photocatalytic nitrogen fixation to ammonia over bismuth monoxide quantum dots-modified defective ultrathin graphitic carbon nitride," *Chemical Engineering Journal*, vol. 406, article 126868, 2021.

[42] W. Yang, H. Zhang, J. Lai et al., "Carbon dots with red-shifted photoluminescence by fluorine doping for optical bio-imaging," *Carbon*, vol. 128, pp. 78–85, 2018.

[43] R. Paleckiene, A. Sviklas, and R. Slinksiene, "Reaction of urea with citric acid," *Russian Journal of Applied Chemistry*, vol. 78, no. 10, pp. 1651–1655, 2005.

[44] S. Huang, Y. Li, Y. Feng et al., "Nitrogen and fluorine co-doped graphene as a high-performance anode material for lithium-ion batteries," *Journal of Materials Chemistry A*, vol. 3, no. 46, pp. 23095–23105, 2015.

[45] Y. N. Sun, J. Q. Yang, and B. H. Han, "Synergetic contribution of nitrogen and fluorine species in porous carbons as metal-free and bifunctional oxygen electrocatalysts for zinc-air batteries," *Applied Catalysis B: Environmental*, vol. 297, article 120448, 2021.

[46] H. Wu, W. Sun, J. Shen, D. Rooney, Z. Wang, and K. Sun, "Role of flower-like ultrathin Co_3O_4 nanosheets in water splitting and non-aqueous Li–O_2 batteries," *Nanoscale*, vol. 10, no. 21, pp. 10221–10231, 2018.

[47] H. Wang, Y. Yang, Y. Liang et al., "Rechargeable Li–O_2 batteries with a covalently coupled $MnCo_2O_4$–graphene hybrid as an oxygen cathode catalyst," *Energy & Environmental Science*, vol. 5, no. 7, pp. 7931–7935, 2012.

[48] Y. Zhu, S. Liu, C. Jin, S. Bie, and J. Wu, "MnO_x decorated CeO_2 nanorods as cathode catalyst for rechargeable lithium–air batteries," *Journal of Materials Chemistry A*, vol. 3, no. 25, pp. 13563–13567, 2015.

[49] Y. Li, L. Zou, and H. Yang, "Synthesis of ordered mesoporous $NiCo_2O_4$ via hard template and its application as bifunctional electrocatalyst for Li-O_2 batteries," *Electrochimica Acta*, vol. 129, pp. 14–20, 2014.

[50] Y. Yang, M. Shi, Q.-F. Zhou, Y. S. Li, and Z. W. Fu, "Platinum nanoparticle-graphene hybrids synthesized by liquid phase pulsed laser ablation as cathode catalysts for Li-air batteries," *Electrochemistry Communications*, vol. 20, pp. 11–14, 2012.

[51] J. Zheng, X. Wu, and Y. Yang, "Improved electrochemical performance of $Li[Li_{0.2}Mn_{0.54}Ni_{0.13}Co_{0.13}]O_2$ cathode material by fluorine incorporation," *Electrochimica Acta*, vol. 105, pp. 200–208, 2013.

[52] L. Li, B. Song, Y. Chang et al., "Retarded phase transition by fluorine doping in Li-rich layered $Li_{1.2}Mn_{0.54}Ni_{0.13}Co_{0.13}O_2$ cathode material," *Journal of Power Sources*, vol. 283, pp. 162–170, 2015.

[53] P. Xu, C. Chen, J. Zhu, J. Xie, P. Zhao, and M. Wang, "RuO_2-particle-decorated graphene-nanoribbon cathodes for long-cycle Li-O_2 batteries," *Journal of Electroanalytical Chemistry*, vol. 842, pp. 98–106, 2019.

[54] H. Lin, Z. Liu, Y. Mao et al., "Effect of nitrogen-doped carbon/Ketjenblack composite on the morphology of Li_2O_2 for high-energy-density Li- air batteries," *Carbon*, vol. 96, pp. 965–971, 2016.